Supplemental Information

Photochemical Cloud Processing of Water-Soluble Organic Gases Produced by Aqueous-Phase Photooxidation of α-Pinene, d-Limonene and Toluene

Matthew L. Zaragoza,[1] Lisa M. Wingen,[1] Sergey A. Nizkorodov,[1,*] and Annmarie G. Carlton[1,*]

[1] *Department of Chemistry, University of California, Irvine, Irvine, CA 92697, United States*

* Corresponding authors' emails: nizkorod@uci.edu and agcarlto@uci.edu

Table of Contents

1. Optimizing WSOG Production from the OFR

Copper tubing wrapped in heating tape was added after the Teflon filters to scrub O_3 from the gaseous oxidation products. This was done to ensure oxidation of WSOGs by the residual O_3 would not occur during the sample collection process, which could have artificially inflated the aqSOA mass. With the heated copper tubing installed, the O_3 was reduced from ~12 ppm to <0.1 ppm, as measured with a home-made spectrophotometric O_3 detector.

To test for unoxidized VOCs exiting the OFR, gas cartridges sampled α-pinene exiting the OFR with and without the O_3 and •OH lamps on. The gas cartridges were stainless steel tubes packed with separate sections of Tenax TA and Carbograph 5TD (Markes, Part C2-AXXXX-5149). The adsorbed organics were thermally desorbed into the Gas Chromatography-Mass Spectrometer to detect α-pinene exiting the OFR. Approximately 2% of α-pinene was found to remain unoxidized after the OFR. Any remaining α-pinene was not thought to significantly affect the experiment because it has a low Henry's law constant of 5.7×10^{-2} M atm^{-1},[1,2] so a negligible amount partitioned into mist chamber WSOG samples. The other two VOCs are expected to have had similar recovery rates exiting the OFR and are also poorly water-soluble in their unoxidized state.

Particle breakthrough of the 0.2 μm Teflon filters was measured using the SMPS in a separate experiment. The particle mass concentration after both Teflon filters was below the detection limit of SMPS, suggesting particle retention efficiency in excess of 99.9%. This control experiment was conducted with α-pinene under the same OFR parameters used in the main experiments.

2. Experimental Diagrams

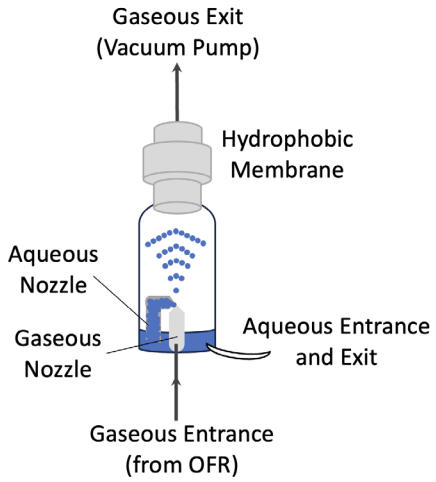

Figure S1: Diagram of the mist chamber. Neat water was added by the side extension, which was part of the custom glassware and partially fills the mist chamber. Gas flowed from the bottom of the mist chamber up through the straight glass nozzle where it intersected with the hooked glass nozzle. The hooked glass nozzle pulled water up which sprayed into a fine mist once it intersected with the gas flow. A hydrophobic membrane prevented water droplets from escaping the mist chamber.

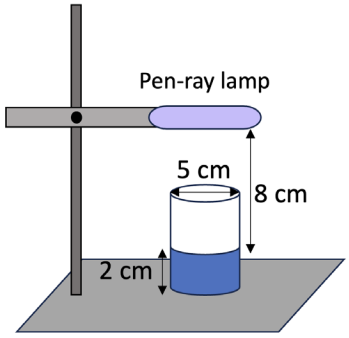

Figure S2: Diagram of the pen-ray lamp setup. Aqueous-phase photooxidation of mist chamber samples was conducted in open room air. A cardboard box was placed over the sample to prevent exposure of experimentalists to UV radiation.

3. Gas-Phase OFR Oxidation

3.1 OFR Oxidant Concentrations

In a separate experiment, a Proton Transfer Reaction-Mass Spectrometer (PTR-MS) measured the •OH concentration during the gas-phase oxidation of toluene in the OFR. The same conditions were applied to this experiment as the experiments in the main text (except that the output of the OFR was diluted with clean air to bring it in range of PTR-MS measurements). Toluene was selected because it was expected to almost exclusively react with •OH. The following equations were used to calculate the •OH exposure and concentration:[3]

$$\bullet OH\ exposure = \frac{-1}{k_{\bullet OH,\ toluene}} \times \ln\left(\frac{[VOC_f]}{[VOC_i]}\right) \quad \text{(S1)}$$

where VOC_i and VOC_f represent the initial and final VOC concentrations, respectively, and $k_{\bullet OH,\ toluene}$ is the rate constant between •OH and toluene (5.63×10^{-12} cm^3 $molec^{-1}$ s^{-1}).[4] The *m/z* 94 toluene isotope was used for VOC_i and VOC_f instead of the most abundant toluene isotope at *m/z* 93 because the *m/z* 93 peak was saturated in the PTR-MS. This method provided an •OH exposure of 3.7×10^{11} molec s cm^{-3}. The average •OH concentration was estimated using the •OH exposure and residence time:

$$[\bullet OH] = \frac{\bullet OH\ exposure}{residence\ time} \quad \text{(S2)}$$

Using the OFR residence time of 3.3 min, the •OH concentration in the OFR was estimated to be 2×10^9 molec cm^{-3}. Separately, the O_3 concentration was measured to be ~3.0×10^{14} molec cm^{-3} as described in section 1 of the SI.

3.2 Reaction Rates and Lifetimes

The reaction rates and lifetimes for each VOC in the OFR can be calculated for both oxidants. Initial VOC mixing ratios were 8.86 ppm for α-pinene, 8.68 ppm for limonene, and 13.2 ppm for toluene. Rate constants between the VOCs and oxidants were taken from the literature.[4–8] The bimolecular rate equation describes the reaction rate:

$$Rate = k[VOC][Oxidant] \quad \text{(S3)}$$

and the atmospheric lifetime is calculated using:

$$\tau = \frac{1}{k[Oxidant]_0} \quad \text{(S4)}$$

Reaction	Reaction Rate (molec cm^{-3} s^{-1})	Lifetime (s^{-1})
α-pinene + O_3	6.2×10^{12}	47
α-pinene + •OH	2.3×10^{13}	9.4
Limonene + O_3	1.4×10^{13}	21
Limonene + •OH	6.9×10^{13}	3.0
Toluene + O_3	9.8×10^{7}	7.1×10^{6}
Toluene + •OH	3.6×10^{12}	89

Table S1: Reaction rates and lifetimes for O_3 and •OH oxidation in the OFR

Table S1 shows the reaction rates and lifetimes for O_3 and •OH gas-phase oxidation in the OFR. The •OH reactions are approximately 2 and 4 times faster than ozonolysis for α-pinene and limonene, respectively. The reaction with O_3 is negligible in comparison to the reaction with •OH for toluene.

3.3 Ambient Oxidation

Equation (S5) demonstrates the relation between the experimental exposure time to ambient exposure time:

$$[OH]_{exp}t_{exp} = [OH]_{amb}t_{amb} \quad \text{(S5)}$$

where "*exp*" denotes the experimental conditions and "*amb*" represents ambient conditions. Using ambient concentrations of 40 ppb for O_3[9] and 5×10^6 molec cm^{-3} for •OH,[10] VOCs were aged an equivalent of 17 h for O_3 and 22 h for •OH in ambient conditions.

4. Quantifying the Aqueous Photooxidation Rate

4.1 Measurements of $[\bullet OH]_{TA}$ during aqueous-phase photooxidation

Terephthalic acid (TA) was used to determine the steady-state concentration of •OH in solution during aqueous-phase photooxidation. A solution of 7.20×10^{-5} M TA was dissolved in 60.0 mL of neat water spiked with 0.045 M of H_2O_2 and exposed for varying time lengths to the same pen-ray lamp environment as the WSOG samples. After every minute, the lamp was blocked, and a 1.00 mL aliquot was removed for analysis with Ultra-High Pressure Liquid Chromatography - Heated Electrospray Ionization - High Resolution Mass Spectrometry (UHPLC-ESI-HRMS, see section SI 10). The lamp was unblocked to continue aqueous-phase photooxidation, and this process was repeated every minute until 4 min was reached. UHPLC-ESI-HRMS was run for these samples to determine the relative intensities of TA and its •OH oxidation product, 2-hydroxyterephthalic acid (TAOH), for each time interval, which occur through reactions S6 – S9:

$$H_2O_2 + h\nu \rightarrow 2\ \bullet OH \qquad J_{H2O2} \qquad \text{(S6)}$$

$$\bullet OH + H_2O_2 \rightarrow \bullet HO_2 + H_2O \qquad k_{H2O2} \qquad \text{(S7)}$$

$$\bullet OH + TA \rightarrow TAOH \qquad k_{TA} \qquad \text{(S8)}$$

$$\bullet HO_2 + \bullet HO_2\ (+M) \rightarrow O_2 + H_2O_2 \qquad k_{HO2} \qquad \text{(S9)}$$

The appearance of product [TAOH] and decay of [TA] were measured over photooxidation time using a UHPLC-ESI-HRMS and can be represented by the first-order rate equations:

$$[TAOH] = [TA]_0 \times (1 - e^{-k_{eff}t}) \qquad \text{(S10)}$$

and

$$[TA] = [TA]_0 \times e^{-k_{eff}t} \qquad \text{(S11)}$$

where

$$k_{eff} = -k_{TA} \times [\bullet OH]_{TA} \qquad \text{(S12)}$$

Dividing equation (S10) by equation (S11) produces a ratio of [TAOH]/[TA]:

$$\frac{[TAOH]}{[TA]} = \frac{(1-e^{-k_{eff}t})}{e^{-k_{eff}t}} \qquad \text{(S13)}$$

The maximum percent loss of [TA] throughout aqueous-phase photooxidation was of the order of 10% based on chromatographic peak intensity. Therefore, assuming [TA] depletion is minimal ($k_{eff}t << 1$), the exponents reduce to:

$$\frac{[TAOH]}{[TA]} \approx k_{eff}t \quad \text{(S14)}$$

The first order rate constant, k_{eff}, was determined from the slope of the plot [TAOH]/[TA] against time (Figure S3) to be 5.9×10^{-4} s^{-1}. A value of 4.1×10^{9} M^{-1} s^{-1} was used for k_{TA},[11] and $[\bullet OH]_{TA} = 1.4\times10^{-13}$ M at steady-state conditions was determined from equation (S12).

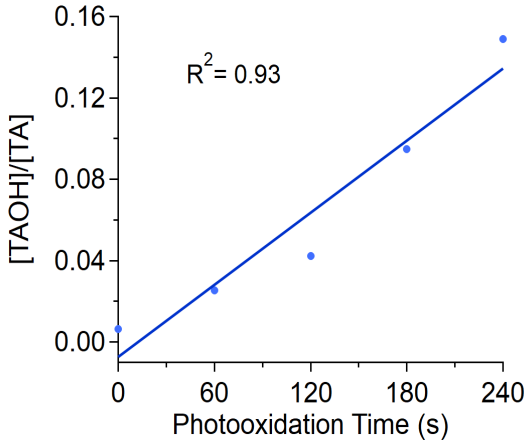

Figure S3: Increase in the hydroxy-terephthalic acid (TAOH) to terephthalic acid (TA) ratio over photooxidation time. The slope of this line was used to determine $[\bullet OH]_{TA}$ in solution.

4.2 Estimation of $[OH]_{WSOG}$ during aqueous-phase photooxidation

Because of the difference in reactivity and WSOG, the •OH concentration measured in presence of terephthalic acid, $[\bullet OH]_{TA}$, needs to be corrected to estimate •OH concentration measured in presence of WSOG, $[\bullet OH]_{WSOG}$. The following set of calculations convert $[\bullet OH]_{TA}$ to $[\bullet OH]_{WSOG}$. Assuming steady-state conditions from equations (S6 – S9) for [•OH] gives:

$$\frac{d[OH]}{dt} = 2J_{H2O2}[H_2O_2] - k_{H2O2}[\bullet OH][H_2O_2] - k_{TA}[\bullet OH][TA] \approx 0 \quad \text{(S15)}$$

Solving for the steady-state $[\bullet OH]_{WSOG}$ in the terephthalic acid experiment gives:

$$[\bullet OH]_{TA} = \frac{2J_{H2O2}[H_2O_2]}{k_{H2O2}[H_2O_2] + k_{TA}[TA]} \quad \text{(S16)}$$

The steady-state [•OH] can be written in the same manner:

$$[\bullet OH]_{WSOG} = \frac{2J_{H2O2}[H_2O_2]}{k_{H2O2}[H_2O_2] + k_{WSOG}[WSOG]} \quad \text{(S17)}$$

Dividing equation (S17) by equation (S16) provides a ratio of the two [•OH] steady-state concentrations:

$$\frac{[\bullet OH]_{WSOG}}{[\bullet OH]_{TA}} = \frac{k_{H2O2}[H_2O_2] + k_{TA}[TA]}{k_{H2O2}[H_2O_2] + k_{WSOG}[WSOG]} \quad \text{(S18)}$$

Therefore, $[\bullet OH]_{WSOG}$ is estimated by:

$$[\bullet OH]_{WSOG} = \frac{k_{H2O2}[H_2O_2] + k_{TA}[TA]}{k_{H2O2}[H_2O_2] + k_{WSOG}[WSOG]} \times [\bullet OH]_{TA} \quad \text{(S19)}$$

The values for k_{TA}, $[\bullet OH]_{TA}$, and [TA] were determined in section 4.1 to be 4.1×10^{9} M^{-1} s^{-1}, 1.4×10^{-13} M, and 7.20×10^{-5} M, respectively. The value for $[H_2O_2]$ was 0.045 M (as mentioned in the main text). The rate constant k_{H2O2} is 2.7×10^{7} M^{-1} s^{-1}.[11] The general rate constant for dissolved organic carbon 3.8×10^{8} L $(mol\ C)^{-1}$ s^{-1} may be used for k_{WSOG}.[12] The concentration of dissolved WSOG is provided by TOC data in section S6, and converted to the appropriate units using:

$$[WSOG] = 3{,}000 ppb\ C \times \frac{\frac{1\mu g}{L}}{ppb} \times \frac{1\ g}{10^6\ \mu g} \times \frac{1\ mol}{120\ g} = 2.5 \times 10^{-5}\ mol\ C\ L^{-1} \quad \text{(S20)}$$

This conversion is for α-pinene WSOG using an approximate TOC concentration of 3,000 ppb C and a molecular weight of 120 g/mol. The molecular weight of the WSOGs may only be estimated because the ionization efficiencies of the WSOG compounds is unknown. A value of 120 g/mol was chosen for the molecular weight of α-pinene WSOGs because it consists of a mix of small organic acids and larger monomeric species. Using the values provided above, $[\bullet OH]_{WSOG}$ is estimated to be 1.7×10^{-13} M, similar to $[\bullet OH]_{TA} = 1.4\times10^{-13}$ M. The same $[\bullet OH]_{WSOG}$ is calculated to 2 significant figures for limonene and toluene WSOGs using the TOC concentrations from section S6 and a molecular weight of 120 g/mol. Therefore, 1.7×10^{-13} M reasonably describes the $[\bullet OH]_{WSOG}$ for all three WSOGs.

4.3 Potential depletion of H_2O_2 during aqueous-phase photooxidation

After rearrangement of equation (S17), J_{H2O2} may be determined:

$$J_{H2O2} = \frac{[\bullet OH]_{WSOG} \times (k_{H2O2}[H_2O_2] + k_{TA}[TA])}{2[H_2O_2]} \quad \text{(S21)}$$

Using the values from sections 4.1 and 4.2, J_{H2O2} was determined to be 2.9×10^{-6} s^{-1}. With this value of J_{H2O2}, $[H_2O_2]$ is expected to remain approximately constant (<1% loss) over the time period of the aqueous-phase photooxidation experiments.

4.4 Relating experimental to ambient aqueous-phase photooxidation times

Equation S5 can also be used to relate experimental to ambient oxidation times in the aqueous-phase. There is a wide range in ambient •OH concentrations in aqueous environments from 10^{-16} - 10^{-12} M.[13,14] Using a value of 10^{-14} M for ambient aqueous •OH concentrations and the value $[\bullet OH]_{WSOG}$ of $1.7\text{x}10^{-13}$ M determined above, 35 s of experimental •OH exposure would be

equivalent to ~10 min in the ambient environment, and 90 min of experimental •OH exposure would be equivalent to ~25 h in the ambient environment. It should be noted that other aqSOA formation via aqueous-phase photooxidation laboratory studies have used experimental aqueous •OH concentrations between 10^{-11} – 10^{-13} M for reference.[15,16]

5. Mass Yield Calculations

Mass yield sample calculations are shown for α-pinene aqSOA after 90 min aqueous-phase photooxidation.

Yield 1:

Y_1 is a measure of how much dissolved gases are converted into aqSOA, defined as:

$$Y_1 = \frac{\text{Final aqSOA } [\mu g/m^3]}{\text{Initial WSOG } [\mu g/m^3]} \quad \text{(S22)}$$

The numerator is obtained directly from SMPS measurements. For example, the average mass concentration for α-pinene aqSOA at 90 min from the SMPS is 13.3 μg/m^3 (Figure 2 of the main text). The denominator can be determined from the mass of dissolved WSOGs and the volume of air to aerosolize the entire sample, as described below.

It is convenient to start with the mass of the VOC that passed through the OFR. Using an injection rate of 10 μL/h for α-pinene infusion in the OFR, α-pinene density of 0.858 g/cm^3, and 5 min of mist chamber sampling time, the mass of α-pinene used for a single mist chamber cycle is:

$$\frac{10\ \mu L}{h} \times \frac{1\ mL}{10^3\ \mu L} \times \frac{0.858\ g}{1\ mL} \times \frac{10^6\ \mu g}{1\ g} \times \frac{1\ h}{60\ min} \times 5\ min = 715\ \mu g \text{ of } \alpha\text{-pinene} \quad \text{(S23)}$$

While 15.0 mL of H_2O was injected into the mist chamber, only 13.8 mL of H_2O remained due to evaporative loss. Therefore, if all α-pinene partitioned into the aqueous sample, it would have a concentration of:

$$\frac{715\ \mu g}{13.8\ mL} = 51.8\ \mu g/mL \text{ of } \alpha\text{-pinene in } H_2O. \quad \text{(S24)}$$

In terms of carbon mass fraction in solution this would correspond to:

$$51.8\ \text{ppm } \alpha\text{-pinene} \times \frac{120\ g/mol}{136\ g/mol} = 45.7\ \text{ppm C}. \quad \text{(S25)}$$

This is the maximum mass fraction of carbon that can partition into the WSOG sample. The molar mass of α-pinene is represented by 136 g/mol and the molar mass of just the carbon in α-pinene is represented by 120 g/mol. We used total organic carbon (TOC) measurements to determine the actual carbon mass fraction of WSOG. The α-pinene WSOG samples prior to aqueous-phase photooxidation contained TOC values of ~3.0 ppm C. Therefore, the fraction of carbon that is trapped as WSOGs is:

$$\frac{3.0 \text{ ppm C}}{45.7 \text{ ppm C}} = 0.0657 \quad \text{(S26)}$$

Using similar methods, partitioning carbon fractions of 0.0670 and 0.0632 were calculated for limonene and toluene WSOGs, respectively.

We can use these carbon fractions to estimate the mass of dissolved WSOGs, with a correction for organic mass/organic carbon (OM/OC)[17] ratio:

$$\text{OM/OC} = 1 + (16/12) \times (\text{O/C}) + (1/12) \times (\text{H/C}) \quad \text{(S27)}$$

$$0.715 \text{ mg} \times 0.0656 \times (\text{OM/OC}) = 0.124 \text{ mg WSOGs} \quad \text{(S28)}$$

Next the mass of WSOGs can be converted into an air concentration.

The concentration of dissolved WSOGs in 13.8 mL H_2O (reduced from 15.0 mL because of evaporative loss) is:

$$\frac{0.124 \text{ mg}}{13.8 \text{ mL}} = 0.00899 \text{ mg/mL} \quad \text{(S29)}$$

The rate of water loss from the atomizer is 0.0274 g/min, or 0.0274 mL/min, based on Figure S4.

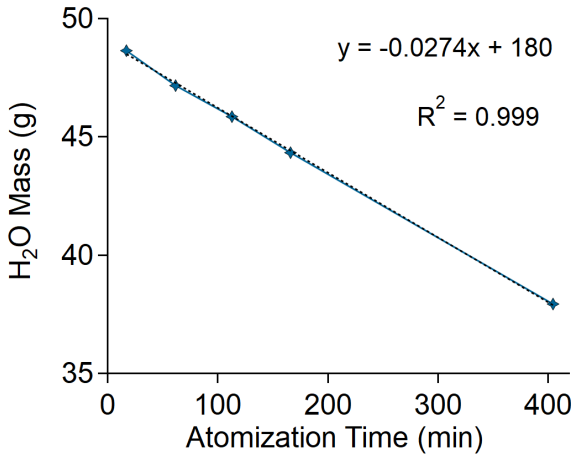

Figure S4: Rate of water mass loss in the atomizer over time.

Using this water loss rate, equation (S29), and an aerosolization rate of 2.00 L/min, the theoretical WSOGs mass concentration can be determined:

$$\frac{0.0274\ \text{mL}\ H_2O}{\text{min}} \times \frac{\text{min}}{2.00\ \text{L air}} \times \frac{10^3\ \text{L}}{\text{m}^3} \times \frac{0.00899\ \text{mg}}{\text{mL}\ H_2O} \times \frac{10^3\ \mu\text{g}}{\text{mg}} = 123\ \mu\text{g WSOG/m}^3\ \text{of air} \quad \text{(S30)}$$

Therefore, the mass yield of aqSOA from α-pinene WSOGs is:

$$Y_1 = \frac{13.3\ \mu\text{g/m}^3}{123\ \mu\text{g/m}^3} = 0.108 \text{ or } 10.8\% \quad \text{(S31)}$$

Yield 2:

The second mass yield shows how much aqSOA is formed from the initial VOC precursor:

$$Y_2 = \frac{\text{Final aqSOA } [\mu\text{g/m}^3]}{\text{Mass of VOC precursor } [\mu\text{g/m}^3]} \quad \text{(S32)}$$

Y_2 considers mass losses from filtering particles, water-insolubilities of organic gases, and incomplete aqueous-phase photooxidation of WSOGs.

The numerator is the mass concentration from the SMPS (13.3 μg/m^3 for this example).

The denominator is obtained by dividing the mass of α-pinene injected into the OFR by the volume of air required to aerosolize all 50.0 mL of the aqSOA sample into the SMPS.

As described above (equation S24), the concentration of α-pinene if it did not react and was fully captured in the WSOG sample is 51.8 µg/mL. Therefore, the total mass for a 50.0 mL sample would be:

$$51.8\ \mu g/mL \times 50.0\ mL = 2{,}590\ \mu g\ of\ \alpha\text{-pinene} \quad (S33)$$

Next the volume of air required to aerosolize all 50.0 mL of WSOG sample is determined using the H_2O aerosolization rate of 0.0274 mL H_2O min^{-1}:

$$50.0\ mL\ H_2O \times \frac{1\ min}{0.0274\ mL\ H_2O} \times \frac{2.00\ L\ air}{min} \times \frac{1\ m^3}{10^3\ L} = 3.65\ m^3\ air \quad (S34)$$

Thus, the hypothetical mass concentration of α-pinene in air would be:

$$\frac{2{,}590\ \mu g}{3.65\ m^3} = 710\ \mu g\ \alpha\text{-pinene}/m^3\ of\ air \quad (S35)$$

Therefore, the aqSOA mass yield from α-pinene is:

$$Y_2 = \frac{13.3\ \mu g/m^3}{710\ \mu g/m^3} = 0.018\ or\ 1.8\% \quad (S36)$$

6. TOC Measurements

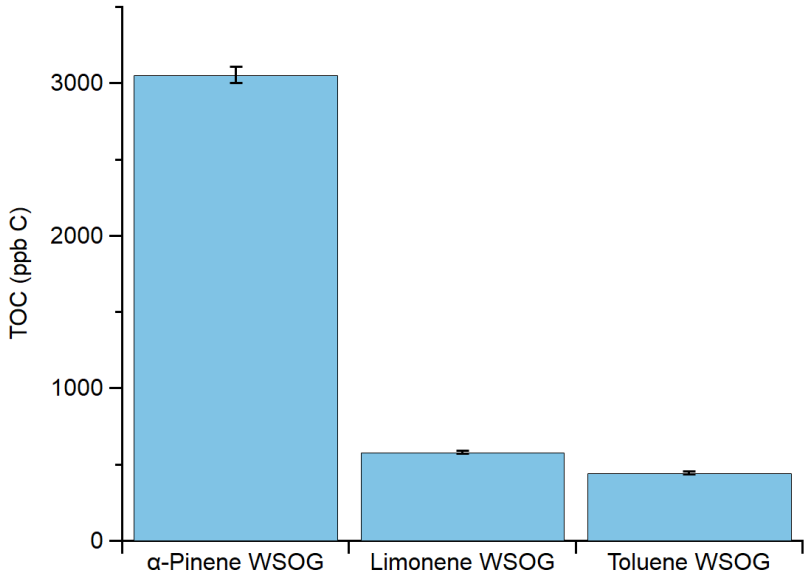

Figure S5: TOC measurements of the three types of WSOG samples. Error bars represent 3 standard deviations.

Total organic carbon (TOC) measurements for the three WSOG types prior to aqueous-phase photooxidation are displayed in Figure S5. Measurements were taken with a Sievers M9 TOC Analyzer. The TOC was operated in grab mode. Blank TOC measurements produced values <10 ppb C. WSOG samples were collected from a separate set of OFR and mist chamber samples, so the TOC concentrations may differ from those of the three sets of samples used to produce Figures 2 in the main text due to variability in the OFR output.

7. Volatility Distributions

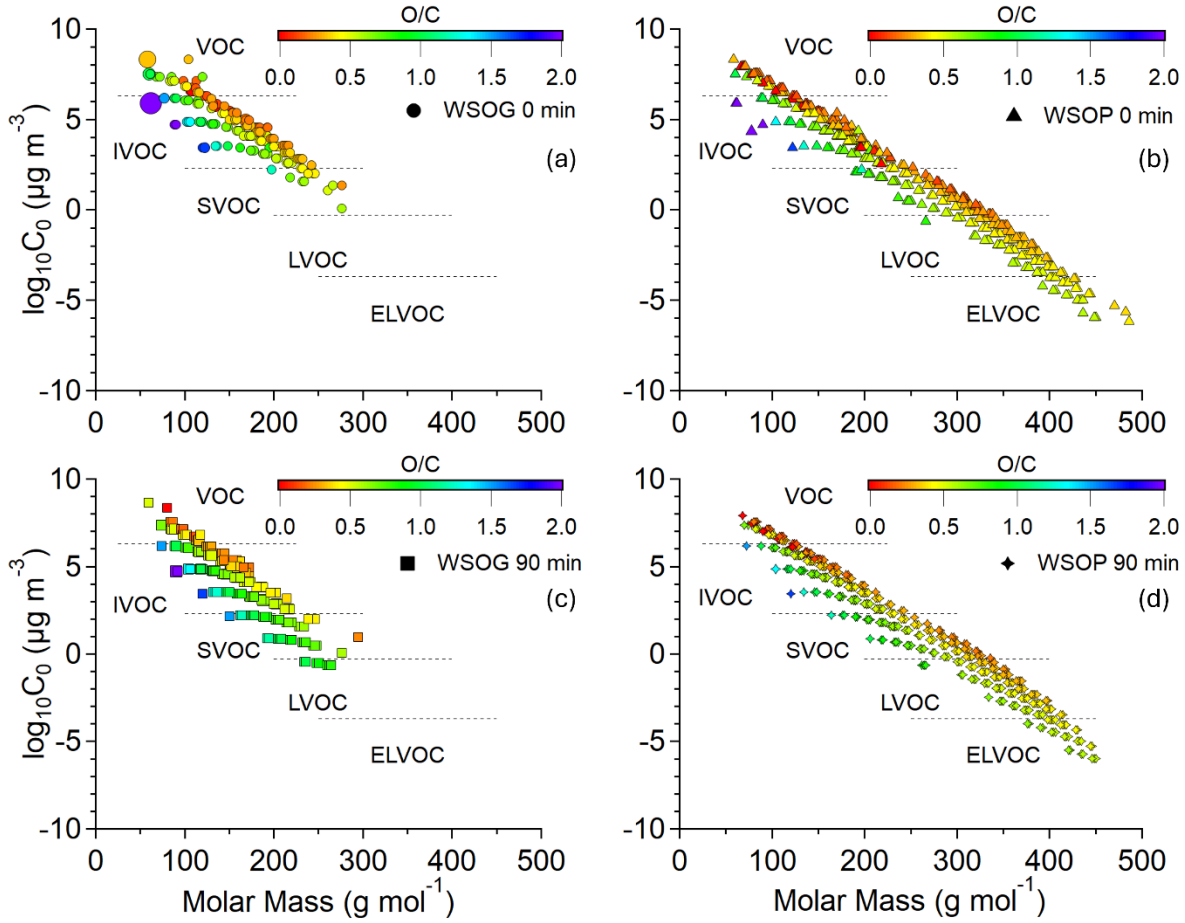

Figure S6: Predicted volatility distributions of WSOGs and WSOPs. Panels **(a)** and **(c)** are for WSOG samples while panels **(b)** and **(d)** are for WSOP samples. Panels **(a)** and **(b)** show samples before aqueous-phase photooxidation and panels **(c)** and **(d)** show samples after 90 min aqueous-phase photooxidation. For each panel, ESI (+) and ESI (-) data were combined into the neutral molar mass represented on the x-axis. The size of each marker represents the intensity of the species in its respective ESI mode before neutral mass combination. The O/C ratios are shown on the color scale ranging from 0-2.0, with O/C capped at 2.0 for species with higher O/C.

Predicted volatility distributions for WSOGs and WSOPs before and after aqueous-phase photooxidation are shown in Figure S6. The predicted volatilities are described by the pure compound saturation mass concentration (C_0) as calculated using the methods described by Li et al.[18] for CHO compounds and equation (S37):

$$log_{10}C_0 = (n_C^0 - n_C)b_C - n_O b_O - 2\,\frac{n_C n_O}{n_C + n_O} b_{CO} \qquad \text{(S37)}$$

Where n_C and n_O are the numbers of carbon and oxygen atoms in the compound, respectively. The CHO parameters n_C^0 b_C, b_O, and b_{CO} are set to values of 22.66, 0.4481, 1.656, and -0.7790, respectively. It should be noted that these volatility distributions are in the absence of non-volatile cations, which are ubiquitous in cloud droplets.

8. Control Experiments

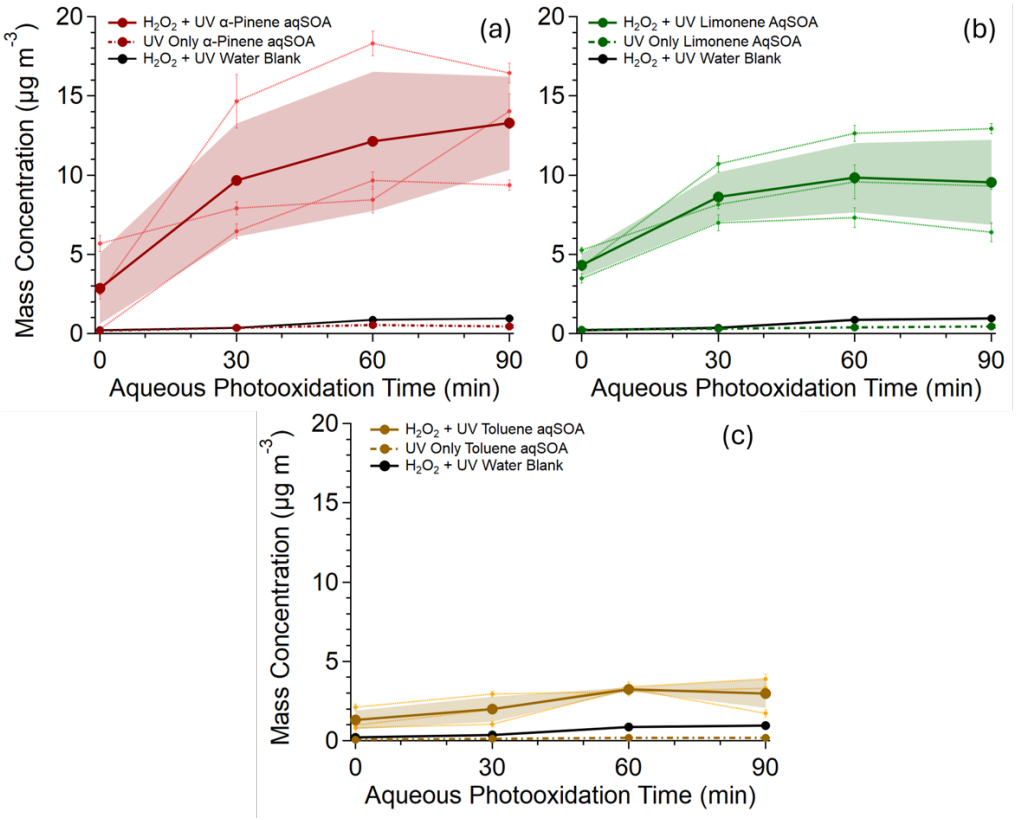

Figure S7: Particle mass concentrations generated from WSOG exposure to UV + H_2O_2 (colored trace), WSOG only exposed to UV (dashed trace), and a water blank (no WSOG) exposed to both UV + H_2O_2 (black trace). One standard deviation is shown by the shading for the WSOG exposed to UV + H_2O_2. Error bars represent one standard deviation for the other samples, which were too small to appear visibly on the graphs, but present. Panels **(a)**, **(b)**, and **(c)**, are separated into the aqSOA and controls for α-pinene, limonene, and toluene WSOGs, respectively.

Figure S7 compares WSOG samples exposed to H_2O_2 + UV irradiation (solid colored trace) to WSOG samples only exposed to only UV irradiation without any added H_2O_2 (dashed colored trace) and a water blank (no WSOG added) exposed to H_2O_2 + UV irradiation (black trace). Less than 1 µg m^{-3} of aqSOA was generated from WSOG exposed to only UV irradiation, indicating that both UV irradiation and H_2O_2 were required to generate aqSOA. Separately, a UV + H_2O_2 water blank underwent a slight mass increase, but also remained under 1 µg m^{-3}. Any particle mass generated was likely due to impurities in the H_2O_2 solution. The H_2O_2 used was 30% ACS grade, but contained inorganic ions that may have served as seeds for particulate mass and organic matter that could have undergone aqueous-phase photooxidation.

9. WSOG Partitioning Behavior

This section discusses different factors that may affect the partitioning behavior of WSOGs. The gas to aqueous-phase partitioning in the mist chamber experiments did not necessarily occur at equilibrium and were thus considered as a function of time. The following differential equation describes the partitioning rate for an atmospheric aqueous droplet:[19]

$$\frac{dC_{aq}}{dt} = k_{mt} LWC (C_g - \frac{C_{aq}}{LWCK_HRT}) \quad \text{(S38)}$$

Concentrations in both gas and aqueous phases are expressed in units of mol g^{-1} air. The differential equation depends on LWC [vol vol^{-1}], the mass transfer coefficient (k_{mt}) [s^{-1}], T [K], R [L atm mol^{-1} K^{-1}], and K_H [mol L^{-1} atm^{-1}]. Values for k_{mt} are determined by:

$$k_{mt} = (\frac{r_d^2}{3D_g} + \frac{r_d}{3\alpha} \times \sqrt{\frac{2\pi M_g}{RT}})^{-1} \quad \text{(S39)}$$

where r_d [m] is the droplet radius, D_g [m^2 s^{-1}] is the diffusion coefficient, M_g [kg mol^{-1}] is the molar mass, and α [unitless] is the mass accommodation coefficient. Solving equation (S38) provides:

$$C_{aq}(t) = C_g LWCK_HRT + Cexp(-\frac{k_{mt}}{K_HRT} \times t) \quad \text{(S40)}$$

Where C is the integration constant. Using the case of $C_{aq} = 0$ at $t = 0$ gives:

$$C = -C_g LWCK_HRT \quad \text{(S41)}$$

Therefore,

$$C_{aq}(t) = C_g LWCK_HRT(1 - exp(-\frac{k_{mt}}{K_HRT} \times t)) \quad \text{(S42)}$$

The aqueous-phase concentration can then be normalized to the volume in the aqueous-phase (instead of volume in the gas-phase):

$$[X]_{aq}(t) = C_g K_HRT(1 - exp(-\frac{k_{mt}}{K_HRT} \times t)) \quad \text{(S43)}$$

In the limit where $\frac{k_{mt}}{K_HRT} \times t \gg 1$, the exponent approaches 0 and the equation reduces to Henry's law equilibrium (since $p_g = C_gRT$):

$$[X]_{aq}(t) = p_g K_H \quad \text{(S44)}$$

Conversely, in the limit where $\frac{k_{mt}}{K_HRT} \times t \ll 1$, corresponding to very large K_H and short sampling time, the concentration increases as a linear function of time.

$$[X]_{aq}(t) = C_g k_{mt} t \quad \text{(S45)}$$

Importantly, the aqueous-phase mass concentrations do not depend on LWC, so the mass concentrations achieved in the mist chamber droplets should be a reasonable representation of what happens in a cloud, despite clouds having much lower LWC compared to the mist chamber. However, the equilibrium is never achieved for compounds with large K_H , leading to differences between resulting concentrations in cloud water and mist chamber, as illustrated below.

The WSOG partitioning behavior in mist chamber and ambient cloud droplets were compared by forming a mass concentration ratio between the droplets in the mist chamber and an ambient cloud droplet. Three representative organic species with different K_H values were used. A temperature of 298 K was used in both scenarios. A droplet radius of 5 μm was used for the mist chamber.[20] A radius of 20 μm was used for a representative ambient cloud droplet in this comparison, although their sizes vary.[19] Literature values for K_H, M_g, D_g, and α are shown in Table S2.[2,21–24]

Parameters	K_H (mol L^{-1} atm^{-1})	M_g (kg mol^{-1})	D_g (m^2 s^{-1})	α
Acetone	2.5×10^{1}	0.058	1.1×10^{-5}	0.066
Acetic Acid	4.0×10^{3}	0.060	1.1×10^{-5}	0.17
Pinonic Acid	2.0×10^{7}	0.184	5.7×10^{-6}	1

Table S2: Parameters used for calculating the aqueous-phase mass concentrations of the three organic species in both mist chamber and ambient cloud droplet scenarios.

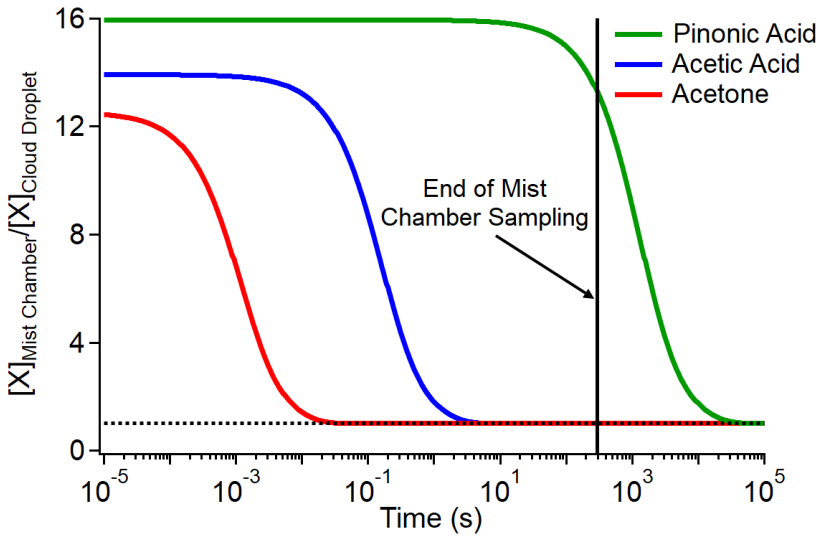

Figure S8. Aqueous-phase mass concentration ratios as a function of partitioning time for three different organic species. The mass concentration in a mist chamber droplet was divided by the mass concentration for a representative ambient cloud droplet to generate the ratio shown on the y-axis. The dashed horizontal line represents when both mass concentrations are equal. The vertical solid line represents t = 300 s, which was the end of mist chamber sampling.

Figure S8 shows the ratio of the aqueous-phase mass concentrations between the mist chamber scenario and the cloud droplet scenario as a function of partitioning time for three different organic compounds. When the exponential term in equation (S41) approaches 0, the equation reduces to Henry's law equilibrium and the $[X]_{Mist\ Chamber}/[X]_{Cloud\ Droplet}$ ratio is equal to 1. Species with larger K_H values take longer to reach equilibrium than species with smaller K_H values. This figure also demonstrates how the WSOG composition will be different between mist chamber droplets and cloud droplets at the beginning of WSOG partitioning. Low K_H species will quickly partition in the same manner for both two scenarios, whereas high K_H species will preferentially partition into mist chamber droplets. The aqueous droplet radius was primarily responsible for the differences in partitioning due to different k_{mt} values.

10. Instrument Measurement Parameters

SMPS

Low-flow mode was used to capture particles between 15-670 nm and scan times for SMPS were 120 s with 30 s of down time in between scans. A density of 1.21 g cm^{-3} for α-pinene SOA,[25] 1.25 g cm^{-3} for limonene SOA,[26–28] and 1.45 g cm^{-3} for toluene SOA[29] were applied.

AMS

A High Resolution Time-of-Flight mass spectrometer (HR-ToF-AMS, Aerodyne) sampled AS-seeded dried aqSOA particles at ~0.08 LPM, vaporized them at ~600°C, and ionized them with electron impact ionization (70 eV)[30]. The AMS was operated in V-mode with a mass resolving power of ~2000, sufficient for separating CHO-containing fragments of the same nominal mass. Purge air was measured to account for gas-phase CO_2 in the air flow before every set of aqSOA measurements. A particle filter was used in a separate experiment during aqSOA sampling to verify that the CO_2^+ fragment intensity was due to aqSOA carboxylic acids and not gas-phase CO_2 being emitted from aqueous samples. When the particle filter was in-line with the atomizer, the CO_2^+ decreased to the same level as clean air, indicating that >99% of the CO_2^+ fragment intensity was due to aqSOA carboxylic acids. Sample collection was split into 80 s of dwell time for MS collection, and 30 s was allocated for PTOF analysis. The software packages SQUIRREL v1.66E and PIKA v1.26E packages within Igor Pro v8.04 were used for high resolution data analysis. A mass range of *m/z* 10-447 was sampled, and the mass range for data analysis was set between *m/z* 12-120.

For AMS experiments, 0.1 mM of AS (Fisher Scientific, 99.0% purity) was added to the atomizer solution so water-soluble organic compounds would adsorb onto AS and allow better transmission into the AMS via >70 nm diameter particles. Approximately 50% of the AS seeded particle mass fell within the measurable diameter range of the AMS. AMS analysis of the organic content of the particles with and without AS was compared in a separate subset of experiments at 30-90 min photooxidation and particles were found to have similar OSc, O/C ratios, and mass spectra. To provide better particle transmission, 0.1 mM AS was added to all solutions going forward. Higher AS concentrations were tested, but were found to interfere with O/C and OSc analysis for some low *m/z* fragments such as CH_3^+. Thus, 0.1 mM AS was chosen because it allowed for enough particle growth required for AMS detection while maintaining consistent elemental composition results to their no AS analogue. The mean geometric diameter

of particles was ~27 nm without AS and ~34 nm with AS. Except for NH_x^+ and SO_y^+ fragments, no significant peaks were observed. Fragments containing both carbon and sulfur were investigated, which might suggest the formation of organosulfur compounds in the presence of AS, but were found to make up <0.2% of the total ion intensity over all experiments.

Separate experiments were conducted using the AMS to measure the O/C ratio of particle oxidation products for comparison to WSOGs for each VOC (section 3.2 of the main text). In these separate experiments, the particles exiting the OFR were sampled by the AMS without the use of a particle filter. A dilution line was also attached to prevent AMS overloading. Data were processed in the same manner as with the aqSOA experiments. Particle O/C ratios had the same results regardless of whether a carbon filter was attached to remove gases.

ESI-HRMS

ESI-HRMS (heated electrospray ionization - Thermo Scientific, Q Exactive Plus Orbitrap high-resolution mass spectrometer) was performed via direct infusion because sample concentrations were too dilute for liquid-chromatography separation, and could not be pre-concentrated by evaporation without loss of volatile sample constituents. Strata-X columns have been used in ambient cloud water studies to concentrate samples, but were not used in this study because they lose small organic acids in the extraction process,[31–35] which are important and abundant analytes in this study. Direct infusion of the sample was performed for 2 min at 35 µL/min in both ESI modes. Data analysis was performed using the "MFAssignR" package in R.[36] All samples were blank subtracted from mist chamber samples that only contained neat water. Because of the low sample concentrations, a signal to noise threshold of 3 was allowed, which is in the lower range of suggested signal to noise ratios. CHON species were allowed to be assigned, but were negligible in data analysis. ESI (-) assignments assumed ionization by the loss of a H^+, while ESI (+) assignments allowed the addition of H^+, Na^+, or NH_4^+ adducts.

UHPLC-ESI-HRMS

Analysis of terephthalic acid and its oxidation product were performed using an UHPLC-ESI-HRMS (Thermo Scientific, Q Exactive Plus Orbitrap high-resolution mass spectrometer coupled to a Vanquish Horizon UHPLC system). Samples were injected in 10 µL aliquots into a Luna Omega 1.6 µm Polar C18 150 × 2.1 mm column (Phenomenex) equipped with a SecurityGuard ULTRA cartridge (porous polar C18, 2.1 mm; Phenomenex), both held at 30°C. The mobile phase flowed at 300 µL min^{-1} and consisted of two solvents. Solvent A was H_2O (Fisher

Chemical, Optima, LCMS grade) containing 0.1% formic acid (Fisher Chemical, Optima, LCMS grade) and solvent B was acetonitrile (Fisher Chemical, Optima, LCMS grade) also containing 0.1% formic acid. The elution used a gradient scheme, which started with 3 min at 5% B, followed by a 14 min linear increase to 95% B, a 2 min hold at 95% B, and finishing with a 6 min return to 5% B. A heated electrospray source (Thermo Scientific) was utilized with a capillary voltage set to 4.0 kV, a capillary temperature maintained at 325°C, a sheath gas flow rate of 35 (arbitrary units; a.u.), an auxiliary gas flow rate of 10 (a. u.), a sweep gas flow rate of 8 (a. u.), an S-lens RF level at 30 (a. u.), and an auxiliary gas heater temperature of 300°C.

11. Cleaning Procedures

After the sample collection for a VOC ended, the Teflon and copper tubing were washed with isopropanol, the OFR was purged with •OH, Teflon filters and hydrophobic filter papers were replaced, and the mist chamber was thoroughly rinsed with neat water. Tubing for water and WSOG sample was rinsed repeatedly with neat water for several hours to remove residual organic compounds. The atomizer and glass jars used to store samples were rinsed with neat water and sonicated for at least 15 min before and after each use to remove residual organic matter and AS.

12. References

(1) Karl, T.; Yeretzian, C.; Jordan, A.; Lindinger, W. Dynamic Measurements of Partition Coefficients Using Proton-Transfer-Reaction Mass Spectrometry (PTR–MS). *International Journal of Mass Spectrometry* **2003**, *223–224*, 383–395. https://doi.org/10.1016/S1387-3806(02)00927-2.

(2) Sander, R. Compilation of Henry's Law Constants (Version 5.0.0) for Water as Solvent. *Atmos. Chem. Phys.* **2023**, *23* (19), 10901–12440. https://doi.org/10.5194/acp-23-10901-2023.

(3) Gu, S.; Khalaj, F.; Perraud, V.; Faiola, C. L. Emerging Investigator Series: Secondary Organic Aerosol Formation from Photooxidation of Acyclic Terpenes in an Oxidation Flow Reactor. *Environ. Sci.: Processes Impacts* **2024**, *26* (7), 1156–1170. https://doi.org/10.1039/D4EM00063C.

(4) Atkinson, R.; Arey, J. Atmospheric Degradation of Volatile Organic Compounds. *Chem. Rev.* **2003**, *103* (12), 4605–4638. https://doi.org/10.1021/cr0206420.

(5) Pate, C. T.; Atkinson, R.; Pitts, J. N. The Gas Phase Reaction of O_3 with a Series of Aromatic Hydrocarbons. *Journal of Environmental Science and Health . Part A: Environmental Science and Engineering* **1976**, *11* (1), 1–10. https://doi.org/10.1080/10934527609385750.

(6) Atkinson, R.; Winer, A. M.; Pitts, J. N. Rate Constants for the Gas Phase Reactions of O3 with the Natural Hydrocarbons Isoprene and α- and β-Pinene. *Atmospheric Environment (1967)* **1982**, *16* (5), 1017–1020. https://doi.org/10.1016/0004-6981(82)90187-1.

(7) Atkinson, R.; Aschmann, S. M.; Pitts, J. N. Rate Constants for the Gas-phase Reactions of the OH Radical with a Series of Monoterpenes at 294 ± 1 K. *Int J of Chemical Kinetics* **1986**, *18* (3), 287–299. https://doi.org/10.1002/kin.550180303.

(8) Khamaganov, V. G.; Hites, R. A. Rate Constants for the Gas-Phase Reactions of Ozone with Isoprene, α- and β-Pinene, and Limonene as a Function of Temperature. *J. Phys. Chem. A* **2001**, *105* (5), 815–822. https://doi.org/10.1021/jp002730z.

(9) Chen, C.; Chen, W.; Guo, L.; Wu, Y.; Duan, X.; Wang, X.; Shao, M. A Comprehensive Review of Tropospheric Background Ozone: Definitions, Estimation Methods, and Meta-Analysis of Its Spatiotemporal Distribution in China. *Atmos. Chem. Phys.* **2025**, *25* (21), 15145–15169. https://doi.org/10.5194/acp-25-15145-2025.

(10) Hewitt, C. N.; Harrison, R. M. Tropospheric Concentrations of the Hydroxyl Radical—a Review. *Atmospheric Environment (1967)* **1985**, *19* (4), 545–554. https://doi.org/10.1016/0004-6981(85)90033-2.

(11) Charbouillot, T.; Brigante, M.; Mailhot, G.; Maddigapu, P. R.; Minero, C.; Vione, D. Performance and Selectivity of the Terephthalic Acid Probe for OH as a Function of Temperature, pH and Composition of Atmospherically Relevant Aqueous Media. *Journal of Photochemistry and Photobiology A: Chemistry* **2011**, *222* (1), 70–76. https://doi.org/10.1016/j.jphotochem.2011.05.003.

(12) Arakaki, T.; Anastasio, C.; Kuroki, Y.; Nakajima, H.; Okada, K.; Kotani, Y.; Handa, D.; Azechi, S.; Kimura, T.; Tsuhako, A.; Miyagi, Y. A General Scavenging Rate Constant for Reaction of Hydroxyl Radical with Organic Carbon in Atmospheric Waters. *Environ. Sci. Technol.* **2013**, *47* (15), 8196–8203. https://doi.org/10.1021/es401927b.

(13) Bianco, A.; Passananti, M.; Brigante, M.; Mailhot, G. Photochemistry of the Cloud Aqueous Phase: A Review. *Molecules* **2020**, *25* (2), 423. https://doi.org/10.3390/molecules25020423.

(14) Ervens, B.; Turpin, B. J.; Weber, R. J. Secondary Organic Aerosol Formation in Cloud Droplets and Aqueous Particles (aqSOA): A Review of Laboratory, Field and Model Studies. *Atmos. Chem. Phys.* **2011**, *11* (21), 11069–11102. https://doi.org/10.5194/acp-11-11069-2011.
(15) Lamkaddam, H.; Dommen, J.; Ranjithkumar, A.; Gordon, H.; Wehrle, G.; Krechmer, J.; Majluf, F.; Salionov, D.; Schmale, J.; Bjelić, S.; Carslaw, K. S.; El Haddad, I.; Baltensperger, U. Large Contribution to Secondary Organic Aerosol from Isoprene Cloud Chemistry. *Sci. Adv.* **2021**, *7* (13), eabe2952. https://doi.org/10.1126/sciadv.abe2952.
(16) Tomaz, S.; Cui, T.; Chen, Y.; Sexton, K. G.; Roberts, J. M.; Warneke, C.; Yokelson, R. J.; Surratt, J. D.; Turpin, B. J. Photochemical Cloud Processing of Primary Wildfire Emissions as a Potential Source of Secondary Organic Aerosol. *Environ. Sci. Technol.* **2018**, *52* (19), 11027–11037. https://doi.org/10.1021/acs.est.8b03293.
(17) Turpin, B. J.; Lim, H.-J. Species Contributions to PM2.5 Mass Concentrations: Revisiting Common Assumptions for Estimating Organic Mass. *Aerosol Science and Technology* **2001**, *35* (1), 602–610. https://doi.org/10.1080/02786820119445.
(18) Li, Y.; Pöschl, U.; Shiraiwa, M. Molecular Corridors and Parameterizations of Volatility in the Chemical Evolution of Organic Aerosols. *Atmos. Chem. Phys.* **2016**, *16* (5), 3327–3344. https://doi.org/10.5194/acp-16-3327-2016.
(19) Ervens, B. Average Cloud Droplet Size and Composition: Good Assumptions for Predicting Oxidants in the Atmospheric Aqueous Phase? *J. Phys. Chem. A* **2022**, *126* (44), 8295–8304. https://doi.org/10.1021/acs.jpca.2c05527.
(20) Stratton, W. J.; Lindberg, S. E.; Perry, C. J. Atmospheric Mercury Speciation: Laboratory and Field Evaluation of a Mist Chamber Method for Measuring Reactive Gaseous Mercury. *Environ. Sci. Technol.* **2001**, *35* (1), 170–177. https://doi.org/10.1021/es001260j.
(21) Seinfeld, J. H.; Pandis, S. N. *Atmospheric Chemistry and Physics: From Air Pollution to Climate Change*, 1st ed.; New York Academy of Sciences Series; John Wiley & Sons, Incorporated: Newark, 2016.
(22) Eyglunent, G.; Le Person, A.; Dron, J.; Monod, A.; Voisin, D.; Mellouki, A.; Marchand, N.; Wortham, H. Simple and Reversible Transformation of an APCI/MS/MS Into an Aerosol Mass Spectrometer: Development and Characterization of a New Inlet. *Aerosol Science and Technology* **2008**, *42* (3), 182–193. https://doi.org/10.1080/02786820801922946.
(23) Gibson, L. T.; Cooksey, B. G.; Littlejohn, D.; Tennent, N. H. Determination of Experimental Diffusion Coefficients of Acetic Acid and Formic Acid Vapours in Air Using a Passive Sampler. *Analytica Chimica Acta* **1997**, *341* (1), 1–10. https://doi.org/10.1016/S0003-2670(96)00566-1.
(24) Shiraiwa, M.; Pöschl, U. Mass Accommodation and Gas–Particle Partitioning in Secondary Organic Aerosols: Dependence on Diffusivity, Volatility, Particle-Phase Reactions, and Penetration Depth. *Atmos. Chem. Phys.* **2021**, *21* (3), 1565–1580. https://doi.org/10.5194/acp-21-1565-2021.
(25) Alla Zelenyuk; Juan Yang; Chen Song; Rahul A. Zaveri; Dan Imre. A New Real-Time Method forDetermining Particles' Sphericityand Density: Application to Secondary Organic Aerosol Formedby Ozonolysis of r-Pinene. *Environ. Sci. Technol.* **2008**, *42* (21). https://doi.org/10.1021/es8013562.
(26) Saathoff, H.; Naumann, K.-H.; Möhler, O.; Jonsson, Å. M.; Hallquist, M.; Kiendler-Scharr, A.; Mentel, Th. F.; Tillmann, R.; Schurath, U. Temperature Dependence of Yields of

Secondary Organic Aerosols from the Ozonolysis of α-Pinene and Limonene. *Atmos. Chem. Phys.* **2009**, *9* (5), 1551–1577. https://doi.org/10.5194/acp-9-1551-2009.
(27) Chen, F.; Zhou, H.; Gao, J.; Hopke, P. K. A Chamber Study of Secondary Organic Aerosol (SOA) Formed by Ozonolysis of d-Limonene in the Presence of NO. *Aerosol Air Qual. Res.* **2017**, *17* (1), 59–68. https://doi.org/10.4209/aaqr.2016.01.0029.
(28) Pytel, K.; Zabiegała, B. Investigation of RH Effect on Uncommon Limonene Ozonolysis Products and SOA Formation in Indoor Air with Real Time Measurement Techniques. *Chemosphere* **2024**, *349*, 140854. https://doi.org/10.1016/j.chemosphere.2023.140854.
(29) Ng, N. L.; Kroll, J. H.; Chan, A. W. H.; Chhabra, P. S.; Flagan, R. C.; Seinfeld, J. H. Secondary Organic Aerosol Formation from *m* -Xylene, Toluene, and Benzene. *Atmos. Chem. Phys.* **2007**, *7* (14), 3909–3922. https://doi.org/10.5194/acp-7-3909-2007.
(30) DeCarlo, P. F.; Kimmel, J. R.; Trimborn, A.; Northway, M. J.; Jayne, J. T.; Aiken, A. C.; Gonin, M.; Fuhrer, K.; Horvath, T.; Docherty, K. S.; Worsnop, D. R.; Jimenez, J. L. Field-Deployable, High-Resolution, Time-of-Flight Aerosol Mass Spectrometer. *Anal. Chem.* **2006**, *78* (24), 8281–8289. https://doi.org/10.1021/ac061249n.
(31) Zhao, Y.; Hallar, A. G.; Mazzoleni, L. R. Atmospheric Organic Matter in Clouds: Exact Masses and Molecular Formula Identification Using Ultrahigh-Resolution FT-ICR Mass Spectrometry. *Atmos. Chem. Phys.* **2013**, *13* (24), 12343–12362. https://doi.org/10.5194/acp-13-12343-2013.
(32) Cook, R. D.; Lin, Y.-H.; Peng, Z.; Boone, E.; Chu, R. K.; Dukett, J. E.; Gunsch, M. J.; Zhang, W.; Tolic, N.; Laskin, A.; Pratt, K. A. Biogenic, Urban, and Wildfire Influences on the Molecular Composition of Dissolved Organic Compounds in Cloud Water. *Atmos. Chem. Phys.* **2017**, *17* (24), 15167–15180. https://doi.org/10.5194/acp-17-15167-2017.
(33) Bianco, A.; Deguillaume, L.; Vaïtilingom, M.; Nicol, E.; Baray, J.-L.; Chaumerliac, N.; Bridoux, M. Molecular Characterization of Cloud Water Samples Collected at the Puy de Dôme (France) by Fourier Transform Ion Cyclotron Resonance Mass Spectrometry. *Environ. Sci. Technol.* **2018**, *52* (18), 10275–10285. https://doi.org/10.1021/acs.est.8b01964.
(34) Bianco, A.; Riva, M.; Baray, J.-L.; Ribeiro, M.; Chaumerliac, N.; George, C.; Bridoux, M.; Deguillaume, L. Chemical Characterization of Cloudwater Collected at Puy de Dôme by FT-ICR MS Reveals the Presence of SOA Components. *ACS Earth Space Chem.* **2019**, *3* (10), 2076–2087. https://doi.org/10.1021/acsearthspacechem.9b00153.
(35) Sun, W.; Fu, Y.; Zhang, G.; Yang, Y.; Jiang, F.; Lian, X.; Jiang, B.; Liao, Y.; Bi, X.; Chen, D.; Chen, J.; Wang, X.; Ou, J.; Peng, P.; Sheng, G. Measurement Report: Molecular Characteristics of Cloud Water in Southern China and Insights into Aqueous-Phase Processes from Fourier Transform Ion Cyclotron Resonance Mass Spectrometry. *Atmos. Chem. Phys.* **2021**, *21* (22), 16631–16644. https://doi.org/10.5194/acp-21-16631-2021.
(36) Schum, S. K.; Brown, L. E.; Mazzoleni, L. R. MFAssignR: Molecular Formula Assignment Software for Ultrahigh Resolution Mass Spectrometry Analysis of Environmental Complex Mixtures. *Environmental Research* **2020**, *191*, 110114. https://doi.org/10.1016/j.envres.2020.110114.